

GPX3 is a key cholesterol-related gene associated with prognosis and tumor-infiltrating T cells in colorectal cancer

Jiming CHEN^{1,2,3}, Yinhang WU^{1,2,3}, Qing ZHOU^{1,2,3}, Yifei SONG^{1,2,3}, Jing ZHUANG^{1,2,3}, Kongjie LU^{1,2,3,*}, Xi YANG^{1,2,3,*}

¹Huzhou Central Hospital, Affiliated Central Hospital Huzhou University, Zhejiang, China; ²Key Laboratory of Multiomics Research and Clinical Transformation of Digestive Cancer of Huzhou, Zhejiang, China; ³Fifth School of Clinical Medicine of Zhejiang Chinese Medical University, Huzhou Central Hospital, Zhejiang, China

*Correspondence: lukongjie2021@163.com; yangxi19900601@126.com

Received July 4, 2023 / Accepted October 25, 2023

High cholesterol is an important factor inducing colorectal cancer (CRC). The study aims to determine the key genes and regulatory mechanism associated with tumor-infiltrating T cells underlying cholesterol-induced CRC. Gene expression data and clinical data from CRCs in The Cancer Genome Atlas (TCGA) were selected for differential expression and survival analysis. A total of 5,815 DEGs and 21 cholesterol-associated KEGG pathways were identified. Subsequently, 128 CRCs and 127 patients without obvious intestinal lesions were recruited to analyze the relationship between GPX3 expression, cholesterol levels, and pathologic condition. The results showed that the expression of cholesterol-related gene GPX3 was negatively associated with cholesterol level, but positively correlated with Ki-67 proliferation index in CRC. The expression of GPX3 was higher in CRC patients who were in poorly differentiated and advanced stage. In addition, a mice model of high-cholesterol diet intervention was constructed to detect the levels of cholesterol and GPX3 in the peripheral blood of mice, and it was found that the expression level of GPX3 in high-cholesterol mice was lower than that in normal diet mice. CD8⁺ T cells were isolated from the spleen of mice and the T cell surface receptors were detected. It was found that the expression of CD69 in CD8⁺ T cells of mice interfered with the high-cholesterol diet, while the expression of PD1, TIM-3, and CTLA-4 was increased. CD8⁺ T cells were co-cultured with MC38 cells to detect the proliferation rate of CRC cells. The results showed that the tumor cell proliferation ratio in the high cholesterol group was higher than that in the control group. Furthermore, GPX3 downstream genes associated with m6A modification and tumor-infiltrating T cells were screened, and a T cell immune-related ceRNA network was constructed. In total, 53 GPX3 downstream genes associated with m6A modification and tumor-infiltrating T cells were identified. A PPI network that contained 45 nodes and 85 interaction pairs was constructed. The ceRNA network, including 39 miRNA-target and 43 lncRNA-miRNA regulatory pairs, was constructed. In conclusion, GPX3 is a potential target for cholesterol regulation of T cell immunity in CRC.

Key words: colorectal cancer; cholesterol; prognosis; glutathione peroxidase 3; m6A modification; tumor-infiltrating T cells

According to the location of the tumor, colorectal cancer (CRC), the second leading cause of cancer-related death globally [1], can be divided into colon adenocarcinoma (COAD) and rectal adenocarcinoma (READ). Despite the continuous progress of multidisciplinary diagnosis and treatment, the prognosis of CRC patients is still poor, and the 5-year survival rate of patients with stage IV CRC is still less than 20% [2]. The etiology of CRC is complex, involving genetic, environmental, and lifestyle risk factors (such as diet) [3]. In particular, high dietary cholesterol intake may increase the susceptibility to cancer and may even affect the survival of cancer patients. Cholesterol typically accumulates

in various malignant tissues, and higher cholesterol levels may be correlated with cancer development and recurrence [4–6]. Notably, elevated serum cholesterol levels have been reported to be related to a higher risk of CRC [7, 8]. However, the association between cholesterol and CRC, as well as the underlying mechanism, has not been fully clarified.

Given the potential role of cholesterol in cancer development, genes involved in the synthesis, metabolism, and transport of cholesterol have been a research hotspot in recent years. Elevated StARD3 expression promotes the aggressiveness of breast cancer by increasing cholesterol biosynthesis, enhancing Src kinase activity, increasing membrane



cholesterol, and inducing oncogenic signaling [9]. Genetic variants of cholesterol pathway genes, including APOB and CDH13, are associated with survival in non-small cell lung cancer by affecting their gene expression and modulating the synthesis, transport, and metabolism of cholesterol [10]. The combined expression of several cholesterol homeostasis genes, including HMGCR, NR1H3, SREBF2, and NR1H2, is correlated with poor clinical outcomes in CRC [11]. Elucidating the key cholesterol-related genes and their mechanism in CRC will help us better understand the pathogenesis of CRC, which could offer new therapeutic opportunities.

Recent reports suggested that cholesterol can modify tumor T cell function with N6-methyladenosine (m6A) modification. m6A is a prevalent RNA modification that critically affects mRNA stability and translation [12]. Dysregulated m6A modification in several oncogenes or tumor suppressors contributes to tumor proliferation and metastasis [13, 14]. Liu et al. demonstrated that the dysregulation of m6A-related genes, such as METTL3, METTL16, and ALKBH5, was related to the clinical outcomes of CRC patients [15]. Moreover, the ectopic expression of m6A-related genes is associated with the prognosis of pancreatic adenocarcinoma and affects the tumor microenvironment (TME) as well [16]. Infiltrated immune cells within the TME are known to act as key regulators in tumorigenesis [17]. Cholesterol could induce CD8⁺ T cell functional exhaustion in the TME [18]. Therefore, the identification of immune cells and immune-related genes associated with prognosis may facilitate the development of immunotherapies for CRC patients [19]. It has been reported that the cholesterol metabolite 27-hydroxycholesterol could promote the metastasis of breast cancer via its action on immune myeloid cells [20]. It has been found that the cholesterol transporter ABCG1 regulates tumor growth by regulating macrophage function within tumors, which suggests a link between cholesterol homeostasis and cancer [21]. Despite these findings, there is limited information on the association between cholesterol, m6A modification, and immune infiltration in CRC.

In this study, a prognostic cholesterol-related gene, glutathione peroxidase 3 (GPX3) was identified. The relationship between GPX3 expression, cholesterol levels, and pathologic condition in CRC patients was determined. The effects of cholesterol on CD8⁺ T cell exhaustion and the role of GPX3 dysregulation in proliferation, invasion, and migration in CRC were investigated. In addition, GPX3 downstream genes associated with m6A modification and tumor-infiltrating T cells were screened, and a T cell immune-related competing endogenous RNA (ceRNA) network was constructed. A flowchart of our study is presented in Supplementary Figure S1. Our findings will lay a theoretical foundation for elucidating the mechanism of cholesterol-induced CRC from the perspective of immunity and may provide promising targets for the individualized treatment of CRC patients.

Patients and methods

Data acquisition and preprocessing. The RNA-seq data and clinical data for COAD and READ were downloaded from The Cancer Genome Atlas (TCGA) database [22]. In total, 431 samples, including 380 tumor samples and 51 adjacent normal samples, were selected. Based on the platform ID/gene mapping annotation information in the Gencode database [23], Ensembl_ID was converted to Symbol_ID. The expression values of mRNAs were obtained and log₂ was transformed.

Besides, the gene expression profile GSE71187 was downloaded from the Gene Expression Omnibus (GEO) database as a validation dataset, including 99 CRC samples and 12 adjacent normal samples. The data were generated on the GPL6480 Agilent-014850 Whole Human Genome Microarray 4x44K G4112F.

Differential expression analysis. Differentially expressed genes (DEGs) between tumor and adjacent normal samples were analyzed using the limma package (version 3.10.3) [24] in R; The p-value was adjusted using the Benjamini-Hochberg method; DEGs were identified with a cutoff value of adjusted $p < 0.05$ and $|\log \text{fold change (FC)}| > 1$; volcano plots of DEGs were then used for visualization.

Analysis of cholesterol-related DEGs. Cholesterol-related genes in cholesterol-related KEGG pathways were screened using lipid-specific keywords, namely glycolipids, sterol lipids, sphingolipids, fatty acyls, glycerophospholipids, prenol lipids, polyketides, and sacharolipids. By intersecting the DEGs, cholesterol-related DEGs were identified.

Survival analysis. Based on the survival data, such as overall survival (OS) and OS status, tumor samples were divided into high- and low-expression groups according to the median expression value of cholesterol-related DEGs. Kaplan-Meier survival analysis was performed using the survival package (version 2.42-6) [25] in R, and then the log-rank test was processed. The DEGs that were related to cholesterol with $p < 0.01$ were defined as prognostic cholesterol-related DEGs.

Validation of the expression of prognostic cholesterol-related DEGs using the microarray data of GSE71187. The expression levels of the identified prognostic cholesterol-related DEGs were further validated using the expression profile GSE71187. One gene (GPX3), which showed consistent expression patterns in both TCGA dataset and the GSE71187 dataset, was used as the target gene for subsequent analysis.

Patient samples. This study was approved by the Ethics Committee of Zhejiang University Huzhou Hospital (No. 202110018-02) and the Chinese clinical trial registry (<http://www.chictr.org.cn>, ChiCTR2200061039). In total, 128 CRC patients confirmed by pathology were included in the experimental group, and 127 patients without obvious intestinal lesions on colonoscopy were included in the control group. Blood samples were taken from all patients in the fasting

state and centrifuged at 4°C for 20 min, and the serum was collected. Biochemical indicators, such as triglyceride, high- and low-density lipoprotein cholesterol, fatty acid, and total cholesterol levels, were detected in the serum samples of the two groups. Finally, CRC patients were divided into a high cholesterol group (≥ 5.17 mmol/l) and a normal cholesterol group (≤ 5.17 mmol/l) according to their peripheral blood cholesterol level, and 15 cases in each group were randomly selected for the follow-up verification.

Immunofluorescence detection of GPX3 expression.

Immunofluorescence was used to detect and localize the expression of CD8 and GPX3 in tissues. Rabbit Anti-GPX3 (ab275965, Abcam, Cambridge, UK), Mouse Anti-CD8 (66868-1-Ig, Wuhan Sanying Biotechnology Co., LTD, Wuhan, China), TRITC sheep anti-mouse (115-025-062, Jackson ImmunoResearch Laboratories, Inc., Commonwealth of Pennsylvania, USA) and FITC sheep anti-rabbit (111-095-003, Jackson ImmunoResearch Laboratories, Inc., Commonwealth of Pennsylvania, USA) were used in the experiments. Tissues from CRC patients were collected, immediately fixed with 4% paraformaldehyde at 20–25°C for 48 h, routinely dehydrated, and embedded in paraffin. Afterward, the colon cancer tissue was cut into 3.5 μm thick sections. To improve cell permeability, sections were immersed in 4% paraformaldehyde fixative for 30 min and washed 3 times with PBS. Subsequently, the sections were blocked at room temperature after dropping H_2O_2 -methanol solution and being rinsed three times with PBS. About 50–100 μl ready-to-use goat serum was added and incubated at room temperature for 20 min. About 50–100 μl primary antibody was added, incubated at 37°C for 2 h in a wet box, and then washed with PBS. Lately, 50–100 μl corresponding TRITC and FITC (1:100 dilution) secondary antibodies were added, incubated at 37°C for 1 h in the dark, and washed with PBS again. Then, 50–100 μl DAPI staining solution was added to each slide and placed at room temperature. The slides were then mounted with anti-extraction sealing tape. The protein expression was observed with a confocal microscope and photographed for preservation. According to the expression of GPX3, CRC patients were divided into a high GPX3 expression group (greater than 70%) and a GPX3 low expression group (less than 50%).

Immunohistochemical staining of Ki-67 proliferation index. The expression level of Ki-67 was detected by the IHC method. The paraffin sections were pretreated with the HE method, and the sections were placed in a staining box, containing antigen retrieval buffer, and heated for antigen retrieval. The sections were dropped with 3% of H_2O_2 -methanol solution and placed at room temperature, rinsed with PBS, and then blocked by adding goat serum. Antigen-antibody reactions were performed by dropping 50–100 μl primary antibody (diluted 1:50) into the sections. After adding an enhancer, 50 μl universal mouse/rabbit polymer and goat-anti-rabbit (1:200) secondary antibody was dropped. DAB was used to develop the color and observed with a microscope until the staining was complete. After counter-

staining with hematoxylin, the slides were mounted, and then the protein expression was observed with a light microscope.

Immunohistochemical staining of CD8 expression level.

CD8⁺ T cells in paraffin sections were counted by immunohistochemical detection. The sections were dried at 25°C and washed three times with 0.01 mol/l PBS. After that, 50 μl anti-CD8 (SP16) rabbit monoclonal antibody ready-use (ZA-0508, Beijing Zhongshan Jinqiao Biotechnology Co., Ltd., Beijing, China) (PBS dilution ratio 1:200) was added. The specific operations were carried out according to the instructions. Each step was washed with 0.01 mol/LPBS (pH 7.4) for 3 times (5 min for each). Finally, a light microscope was used to observe with a high magnification field (100 \times and 200 \times). Light yellow to tan cytoplasm was CD8 positive cells. At least, 2 pathologists evaluated the percentage of CD8 positive cells.

Establishment of a high-cholesterol mouse model. All procedures, involving experimental mice, were approved by the Huzhou Central Hospital Animal Ethics Committee (No. 202111002). Six-week-old C57/BL6 mice (Beijing Weitong Lihua Experimental Animal Technology Co., Ltd., Beijing, China) were housed under standard conditions (constant temperature (20 \pm 1°C), 50% of humidity, and 12 h light/dark cycle) with free access to water. According to the previous method [26], the AOM/DSS inflammatory-induced mouse model was first established, after which the mice were randomly assigned to the control (n=10) or the high cholesterol (n=10) group. Mice in the high cholesterol group were given basic feed containing 1.25% of cholesterol and 0.5% of bile salts for 3 months, and mice in the control group were given basic feed containing 0.5% of bile salts for 3 months.

Enzyme-linked immunosorbent assay (ELISA). The expression of GPX3 in peripheral blood samples from mice in different groups was detected using an ELISA kit (ALPCO Diagnostics, Salem, NH, USA) following the operation instructions.

Detection of peripheral blood total cholesterol level by enzyme colorimetric assay. Cholesterol levels in the peripheral blood of patients with CRC, high-cholesterol-fed mice, and control mice were measured using an enzymatic cholesterol determination kit (Abbott GmbH & Co. KG, Wiesbaden, Germany) following the protocol provided by the manufacturer. OLYMPUS AU400 automatic biochemical analyzer was selected for the analysis.

Flow cytometric analysis. The spleens of mice were extracted under aseptic conditions, cut into small pieces approximately 1 mm in size, and digested in a solution containing 0.1% collagenase (5 ml) at 37°C. Subsequently, 10 ml of PBS was added to the cell suspension, which was then filtered through a nylon membrane and centrifuged at 300 \times g for 10 min at 4°C. The resulting cell pellet was washed twice with PBS. Following the washing and counting steps, the cells were either immunophenotyped or used for the isolation of CD8⁺ cells, depending on the experimental requirements.

For cell phenotype analysis, cells were incubated with CD69-FITC (Abcam, Cambridge, MA, USA), PD1-PE

(Abcam), CTLA-4-APC (Thermo Fisher Scientific, Waltham, MA, USA), and TIM-3-PE (Thermo Fisher Scientific) for 30 min in the dark. Afterward, 400 μ l of PBS was added, and the fluorescence signals of 10,000 cells in each sample were analyzed using a FACSCalibur flow cytometer (Becton Dickinson, Mountain View, CA, USA) with CellQuest software (Becton Dickinson).

Co-culture of CD8⁺ T cells and CRC cells. The pellet of 10^7 cells was resuspended in 90 μ l of buffer, and 10 μ l of CD8 sorting magnetic beads were added, followed by incubation at 4°C for 15 min. The samples were then washed with PBS, centrifuged at 300 \times g for 7 minutes, and the supernatant was discarded. The cells were re-suspended in 500 μ l of buffer and transferred to a magnetic field for 6–8 minutes. After removing the supernatant, the samples were taken out of the magnetic field, washed again, and finally re-suspended in the washing buffer for future use.

MC38 colon adenocarcinoma cells at the logarithmic proliferation stage were digested with 0.25% of trypsin into a single-cell suspension and plated in the lower chamber of a 6-well plate at a density of 2×10^5 cells/well. CD8⁺ T cells were placed in Transwell culture inserts at the same density. After co-culture in RPMI-1640 medium at 37°C with 5% of CO₂, CD8⁺ T cells in the upper inserts and MC38 cells in the lower inserts were collected for subsequent experiments.

CCK-8 assay for cell proliferation detection. CRC cells from the three groups were digested and suspended. A 200 μ l cell suspension (1×10^5 cells/ml) was plated in a 96-well plate. At the indicated time points, 10 μ l of CCK-8 solution (Beyotime, Jiangsu, China) was added to each well and incubated at 37°C. The optical density at 450 nm wavelength was measured using a microplate reader (Bio-Rad, Hercules, CA, USA).

Association analysis of GPX3 expression and clinical phenotypes. According to the median GPX3 expression, patients were divided into the GPX3 high- and low-expression group. The clinical factors, including gender, age, TNM stage, and pathologic stage between the two groups were analyzed by the chi-squared (χ^2) test. Clinical factors with $p < 0.05$ were associated with GPX3 expression.

Analysis of GPX3-related DEGs. The limma package (version 3.10.3) [23] in R was selected to perform the differential expression analysis between the GPX3 high- and low-expression groups. GPX3-related DEGs were selected with a cutoff value of adjusted $p < 0.05$ and $|\log FC| > 1$.

Identification of m6A target genes. The target genes of m6A were downloaded from the Potential Targets module of the m6A2Target database (<http://m6a2target.canceromics.org>). By intersecting with GPX3-related DEGs, cholesterol-related m6A target genes were identified.

Immune infiltration analysis. Using the RNA-seq data of cholesterol-related m6A target genes, the abundance of 22 types of infiltrating immune cells in tumor tissues was evaluated by the CIBERSORT algorithm [27] with the LM22 signature as a reference. The parameters were set as follows: PERM = 100 and QN = F. Then, the differences in the infil-

tration proportion of immune cells between the GPX3 high- and low-expression groups were compared by t-test using the vioplot (version 0.3.2) package in R. T cells with $p < 0.01$ were selected for subsequent analysis.

Screening of T cell immune-related genes. T cell immune-related genes were further screened by analyzing the correlation between cholesterol-related m6A target genes and T cells using Pearson's correlation coefficient. Finally, the value of p that was less than 0.01 was set as the threshold value for selecting T cell immune-related genes.

Functional enrichment analysis. To clarify the function of T cell immune-related genes, KEGG [28] pathway and GO BP [29] enrichment analyses were performed using cluster Profiler (version 3.16.0) [30]. Count ≥ 2 and $p < 0.05$ indicated enrichment results with a statistical difference.

Construction of the protein-protein interaction (PPI) network. To predict the PPI pairs between T cell immune-related genes, the STRING (version 11.0) database [31] was used. The species was set as human, and the PPI score was 0.4. Finally, the Cytoscape (version 3.6.1) [32] was selected to construct the PPI network.

Construction of the ceRNA network. The miRNAs of genes with a degree > 5 in the PPI network were predicted using miRWalk 2.0 [33, 34]. The miRNA-target gene pairs found in the miRWalk, MicroT4, miRanda, miRDB, RNA22, and Targetscan databases were selected for network construction. Afterward, the miRNA-related lncRNAs were predicted using the Prediction Module of DIANA-LncBase v2 [35], and lncRNA-miRNA regulatory relationships with scores = 1 were obtained. The lncRNA-miRNA-mRNA ceRNA network was constructed by integrating the miRNA-target gene pairs and lncRNA-miRNA regulatory relationships. Furthermore, the network topology properties of nodes, including the node degree, were analyzed using CytoNCA (version 2.1.6) [36].

Statistical analysis. Statistical analysis was performed using SPSS 18.0 (IBM Corp., Armonk, NY, USA). The data are expressed as the mean \pm standard deviation, and differences between groups were analyzed by Student's t-test. The correlation between cholesterol levels and GPX3 expression was evaluated by Pearson's correlation analysis. A value of $p < 0.05$ was considered statistically significant.

Results

GPX3 as a prognostic cholesterol-related DEG in CRC. With a cutoff value of adjusted $p < 0.05$ and $|\log FC| > 1$, 5,815 DEGs between tumors and adjacent normal samples were selected, consisting of 2,191 upregulated genes and 3,624 downregulated ones. A volcano plot of the DEGs is shown in Figure 1A. Using lipid-specific keywords, 21 cholesterol-related KEGG pathways (Supplementary Table S1) corresponding to 555 genes were identified. By further intersecting the DEGs, 197 cholesterol-related DEGs were identified (Figure 1B). Further survival analysis revealed that 6

cholesterol-related DEGs (GPX3, FABP4, PRKG1, PTGIS, TMEM189-UBE2V1, and CPT2) were significantly associated with patient prognosis (Figure 1C). Among them, GPX3 ($p=0.002$), FABP4 ($p=2e-04$), PRKG1 ($p=0.0094$), and PTGIS ($p=0.00081$) were negatively correlated with the good prognosis of CRC, while TMEM189-UBE2V1 ($p=0.0091$) and CPT2 ($p=0.0098$) were positively correlated with the prognosis. The expression levels of the 6 cholesterol-related DEGs were further validated using the expression profile GSE71187 that was downloaded from GEO. The expression patterns of 5 genes were consistent in TCGA and GEO datasets, and only GPX3 was significantly differentially expressed ($|\log FC|>1$) in both datasets (Figure 1D). Therefore, GPX3 was selected for subsequent analyses.

Relationship between GPX3 expression, cholesterol levels, and pathologic condition in CRC patients. The biochemical indicators of patients with CRC and healthy controls are illustrated in Table 1. The levels of TG, LDL, and Tc in CRC patients were higher than those in healthy controls, while the levels of APOA1 and APOE in CRC patients were lower than those in healthy controls. To investigate the correlation between GPX3 expression and cholesterol levels, GPX3 protein expression in cancerous tissues with CRC was determined. The expression of GPX3 was negatively correlated with cholesterol levels ($R^2=0.4667$, $p<0.001$) (Figures 2A, 2B). Moreover, the relationship between GPX3 expression and pathologic condition was further analyzed. The results proved that the expression of GPX3 was higher in CRC patients who were in poorly differentiated and advanced stage (Figures 2C–2E). The expression of GPX3 was positively correlated with the Ki-67 proliferation index in CRC patients (Figures 2F, 2G). Furthermore, the expression of CD8⁺ T cells in the cancerous tissues with different levels of cholesterol was analyzed. The results indicated that the expression level of CD8⁺ T cells in the high cholesterol group was lower than that in the normal cholesterol group (Figures 2H, 2I). The expression of GPX3 in CD8⁺ T cells was lower in cancerous tissues than that in paracancerous tissues (Figures 2J, 2K).

Cholesterol-induced CD8⁺ T cell exhaustion in mice. The cholesterol levels were significantly increased in high-cholesterol-fed mice compared with control mice *in vivo* experiments, which suggested that a high cholesterol model was successfully established (Figures 3A, 3B). Furthermore, ELISA revealed that GPX3 expression was markedly decreased in the peripheral blood samples of high cholesterol mice compared with those of control mice (Figure 3C).

What's more, CD8⁺ T cells were isolated from high cholesterol mice and their cell phenotypes were detected by flow cytometry. The results demonstrated that CD69 expression was significantly decreased in high cholesterol mice compared with control mice, whereas the expression of PD-1, CTLA-4, and TIM-3 was remarkably increased ($p<0.05$, Figure 3D, Supplementary Figure S2), which suggested that high cholesterol-induced CD8⁺ T cell exhaustion.

Moreover, CD8⁺ T cells were co-cultured with MC38 cells to detect the CRC cell proliferation ratio. According to the results, the tumor cell proliferation ratio in the high cholesterol group was higher than that in the control group (Figure 3E). These results revealed that GPX3 may be a potential target for high cholesterol-induced CD8⁺ T cell exhaustion in CRC.

Association of GPX3 expression with the clinical phenotype. To clarify the correlation between GPX3 and clinical phenotype (including age, gender, TNM stage, pathologic stage), patients were divided into two groups with high and low expression according to the median expression of GPX3. The chi-square test was used to calculate p-value, and clinical factors with $p<0.05$ were related to the group. These results illustrated that there were significant differences in GPX3 expression levels in the clinical stage ($p<0.001$), but no differences among gender and age, which suggested the potential of GPX3 in predicting the clinical stage (Table 2).

Table 1. Biochemical indicators of patients with colorectal cancer and healthy controls.

Indicators	Healthy controls ($\bar{x}\pm s$)	CRC ($\bar{x}\pm s$)	t-value	p-value
TG (mmol/l)	1.23±0.16	1.32±0.14	-4.75	<0.001
HDL (mg/dl)	44.24±1.22	43.91±2.69	1.25	0.214
LDL (mg/dl)	98.08±7.15	145.98±5.15	-61.38	<0.001
Tc (mmol/l)	4.15±0.08	4.57±0.23	-19.50	<0.001
LP (a) (g/l)	20.60±1.11	20.37±1.34	1.51	0.133
APOA1 (g/l)	1.44±0.05	0.97±0.04	82.17	0.033
APOB (g/l)	0.95±0.05	0.94±0.04	1.20	0.232
APOE (g/l)	60.74±0.68	45.18±0.10	145.20	<0.001
FFA (mmol/l)	532.40±6.51	533.04±7.72	-0.72	0.474
ALT (IU/l)	22.02±0.70	22.20±0.81	-1.92	0.056
AST (IU/l)	26.33±0.83	26.62±1.50	-1.94	0.054
Glu (mmol/l)	5.46±0.32	5.51±0.35	-1.33	0.186
OT (μmol/l)	11.97±0.18	11.98±0.23	-2.06	0.837
DT (μmol/l)	4.74±0.23	4.78±0.19	-1.18	0.070

Table 2. Analysis of clinical factors associated with GPX3 expression.

Clinical factors	GPX3		p-value
	High-expression group (N=190)	Low-expression group (N=190)	
Gender			1
Female	87.0 (45.8%)	87.0 (45.8%)	
Male	103 (54.2%)	103 (54.2%)	
Age (years)			0.303
<65	93.0 (48.9%)	82.0 (43.2%)	
≥65	97.0 (51.1%)	108 (56.8%)	
Stage			<0.001
NA	10.0 (5.3%)	9.00 (4.7%)	
Stage I	18.0 (9.5%)	38.0 (20.0%)	
Stage II	58.0 (30.5%)	78.0 (41.1%)	
Stage III	73.0 (38.4%)	43.0 (22.6%)	
Stage IV	31.0 (16.3%)	22.0 (11.6%)	

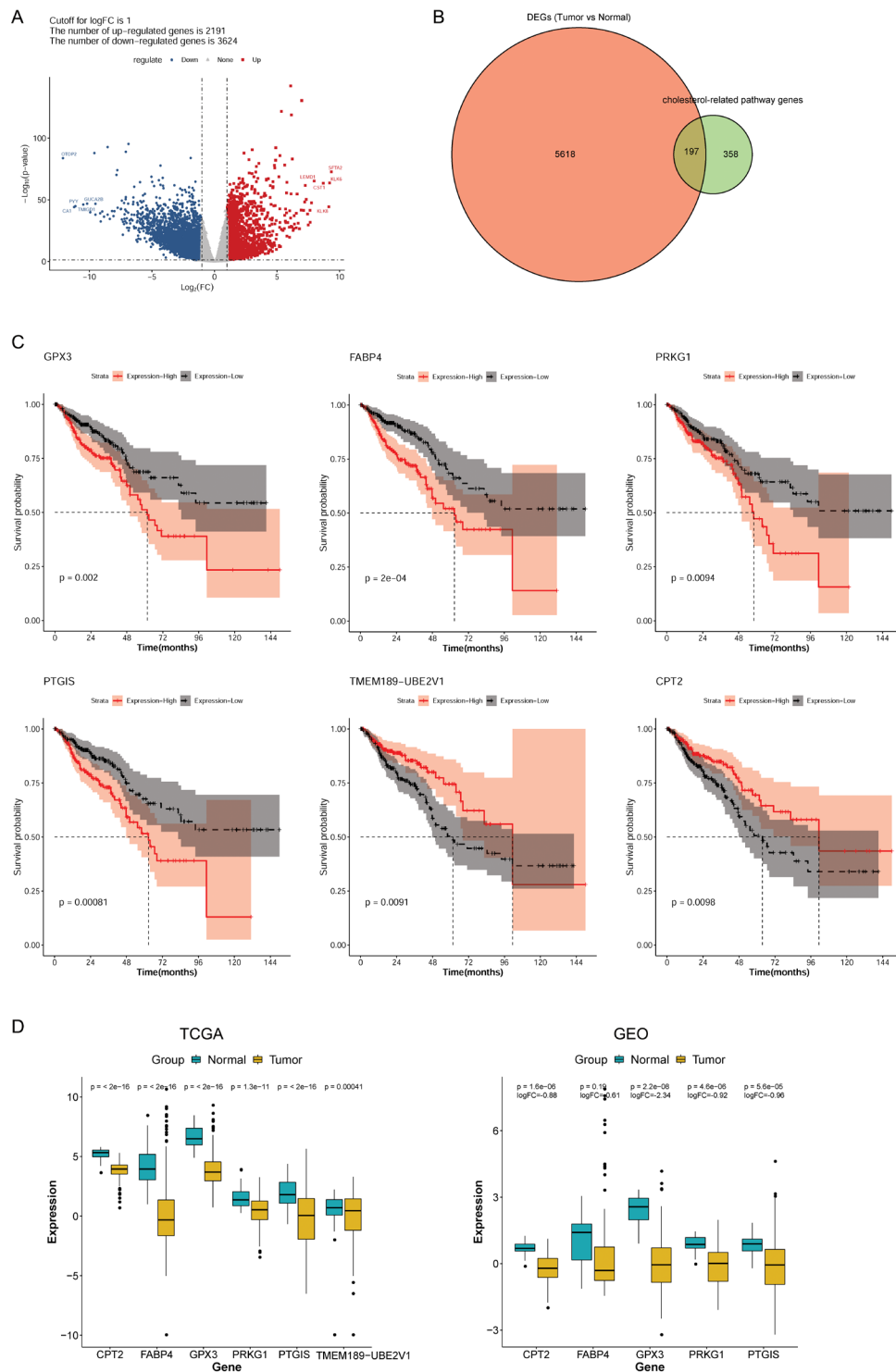


Figure 1. GPX3 as a prognostic cholesterol-related gene in CRC. A) Volcano plot of DEGs between tumor and adjacent normal samples. The red node represents upregulated mRNAs, and the blue node represents downregulated mRNAs. The abscissa axis is the fold change after log₂ conversion (log₂FC), and the longitudinal axis is the p value after log₁₀ conversion, i.e., log₁₀(p-value). B) Venn analysis shows the intersection of DEGs and cholesterol-related pathway genes. C) Kaplan-Meier survival curve analysis shows the prognostic value of 6 cholesterol-related DEGs (GPX3, FABP4, PRKG1, PTGIS, TMEM189-UBE2V1, and CPT2). The abscissa axis is the survival time (months), and the longitudinal axis is the overall survival. The p-value was calculated by the log-rank test. D) Expression boxplots of GPX3, FABP4, PRKG1, PTGIS, TMEM189-UBE2V1, and CPT2 based on TCGA and GEO datasets. Only GPX3 was significantly differentially expressed ($|\log_2 \text{FC}| > 1$) in both datasets. Abbreviations: DEGs-differentially expressed genes; TCGA-The Cancer Genome Atlas; GEO-Gene Expression Omnibus.

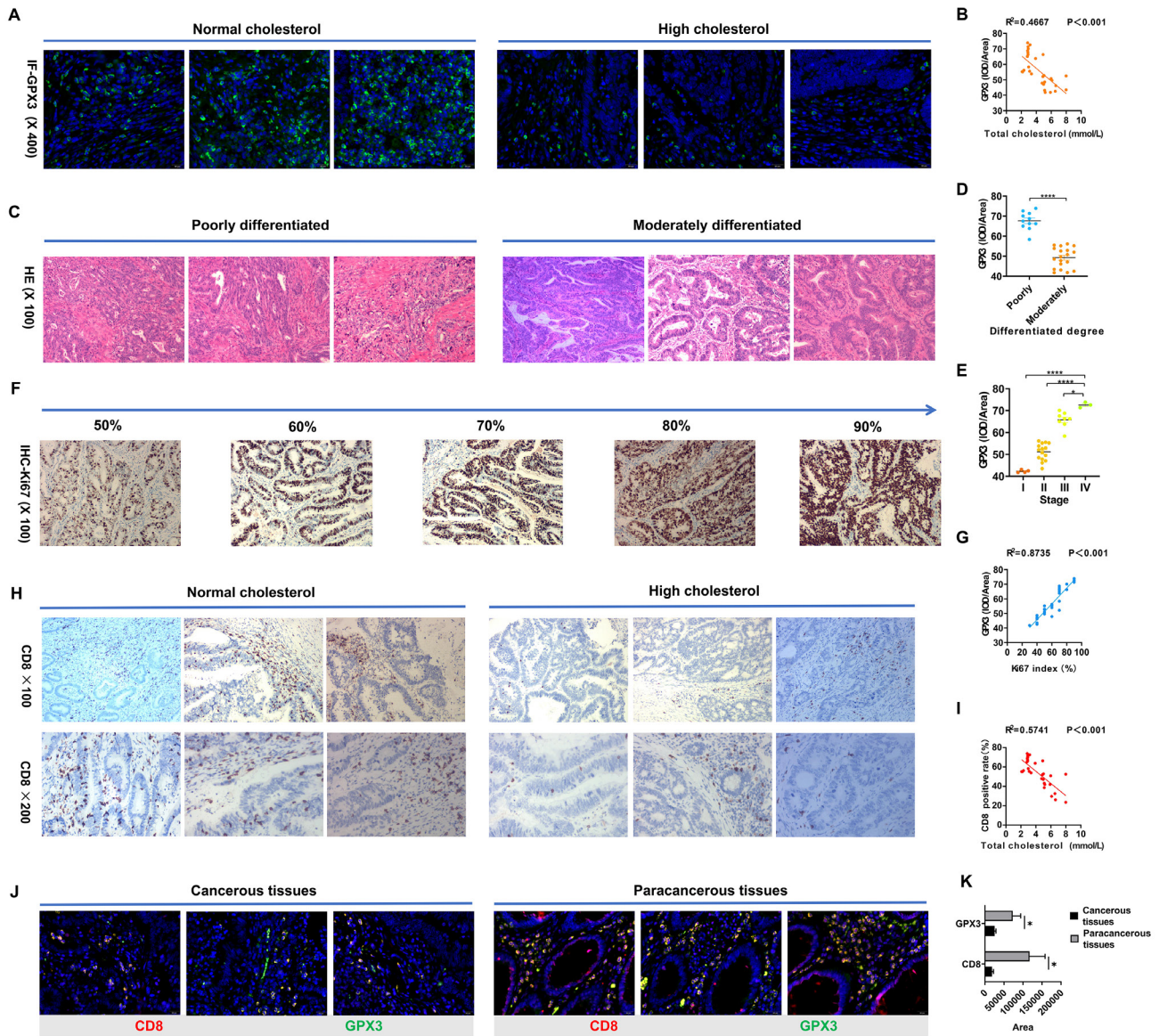


Figure 2. The relationship between GPX3 and peripheral blood cholesterol levels and pathology of CRC. A) Immunofluorescence images of CRC tissues with normal and high cholesterol under 400x microscope. B) Relationship between GPX3 expression level and cholesterol level. C) HE-stained section of poorly and moderately differentiated CRC tissue under 100x microscope. D) Relationship between the expression level of GPX3 and the degree of CRC differentiation. E) Relationship between GPX3 expression level and CRC stage. HE: hematoxylin-eosin staining. F) Immunohistochemical images of the Ki-67 proliferation index increasing from 50-90% under 100x microscope. G) Relationship between GPX3 expression level and the Ki-67 proliferation index. H: Immunohistochemistry detection of CD8⁺ T cells in the CRC cancerous tissues at normal cholesterol level and high cholesterol level. I: The correlation between cholesterol level and CD8 positive proportion was analyzed by linear regression, and Pearson index was calculated. J) Immunofluorescence (IF) detection and localization of CD8 and GPX3 expression in cancer tissues and paracancerous tissues. K) Bar chart of CD8 and GPX3 expression in cancer tissues and paracancerous tissues. *p<0.05

Analysis of GPX3-related DEGs. To further elucidate the regulatory mechanism of GPX3, differential expression analysis between the GPX3 high- and low-expression groups was performed. A total of 2,351 DEGs (2,320 upregulated and 31 downregulated) were identified (Figure 4A). In total, 1,747 target genes of m6A were downloaded from the Potential Targets module of the m6A2Target database. By inter-

secting with GPX3-related DEGs, 59 cholesterol-related m6A target genes were identified (Figure 4B). Moreover, the abundance of 22 types of infiltrating immune cells in tumor tissues was evaluated using the CIBERSORT algorithm. The abundance of 9 infiltrating immune cells showed significant differences between the GPX3 high- and low-expression groups, which included plasma cells, memory CD4 T cells,

activated memory CD4 T cells, follicular helper T cells, M1 macrophages, M2 macrophages, activated dendritic cells, resting mast cells, and activated mast cells (Figure 4C). By analyzing the correlation between cholesterol-related m6A target genes and tumor-infiltrating T cells using Pearson's correlation coefficient, 53 T cell immune-related genes were identified, all of which were upregulated.

Functional enrichment analysis for T cell immune-related genes. To clarify the function of T cell immune-related genes, KEGG pathway and GO BP enrichment analyses were carried out. T cell immune-related genes were significantly enriched in 20 KEGG pathways (such as proteoglycans in cancer, regulation of actin cytoskeleton, and phagosome) and 417 GO BP terms (such as muscle system process, leukocyte migration, and cell-substrate adhesion). The top 10 enrichment results of KEGG pathways and GO BP terms are shown in Figures 5A and 5B, respectively.

PPI network analysis for T cell immune-related genes. Based on the STRING database, a PPI network was

constructed, with 45 nodes and 85 interaction pairs. Nodes with a node degree >5 included FN1 (degree = 19), FLNA (degree = 9), VIM (degree = 8), CAV1 (degree = 8), ACTC1 (degree = 7), TPM2 (degree = 7), ITGA5 (degree = 7), ACTG2 (degree = 6), ICAM1 (degree = 6), and SERPINE1 (degree = 6) (Figure 5C).

Analysis of the T cell immune-related ceRNA network. Using miRWalk 2.0, 62 miRNAs that could target 7 T cell immune-related genes with a degree >5 in the PPI network were identified. ACTC1 (degree = 18) was targeted by the greatest number of miRNAs, followed by SERPINE1 (degree = 16) and FN1 (degree = 11). Seven lncRNAs that could regulate 39 miRNAs were predicted using DIANA-LncBase v2. Among these lncRNAs, chr22-38_28785274-29006793.1 interacted with the greatest number of miRNAs. By integrating the miRNA-target gene pairs and lncRNA-miRNA regulatory relationships, a T cell immune-related ceRNA network was constructed, including 7 lncRNAs, 39 miRNAs, 7 immune-related genes, 39 miRNA-target gene pairs, and 43 lncRNA-miRNA regulatory relationships

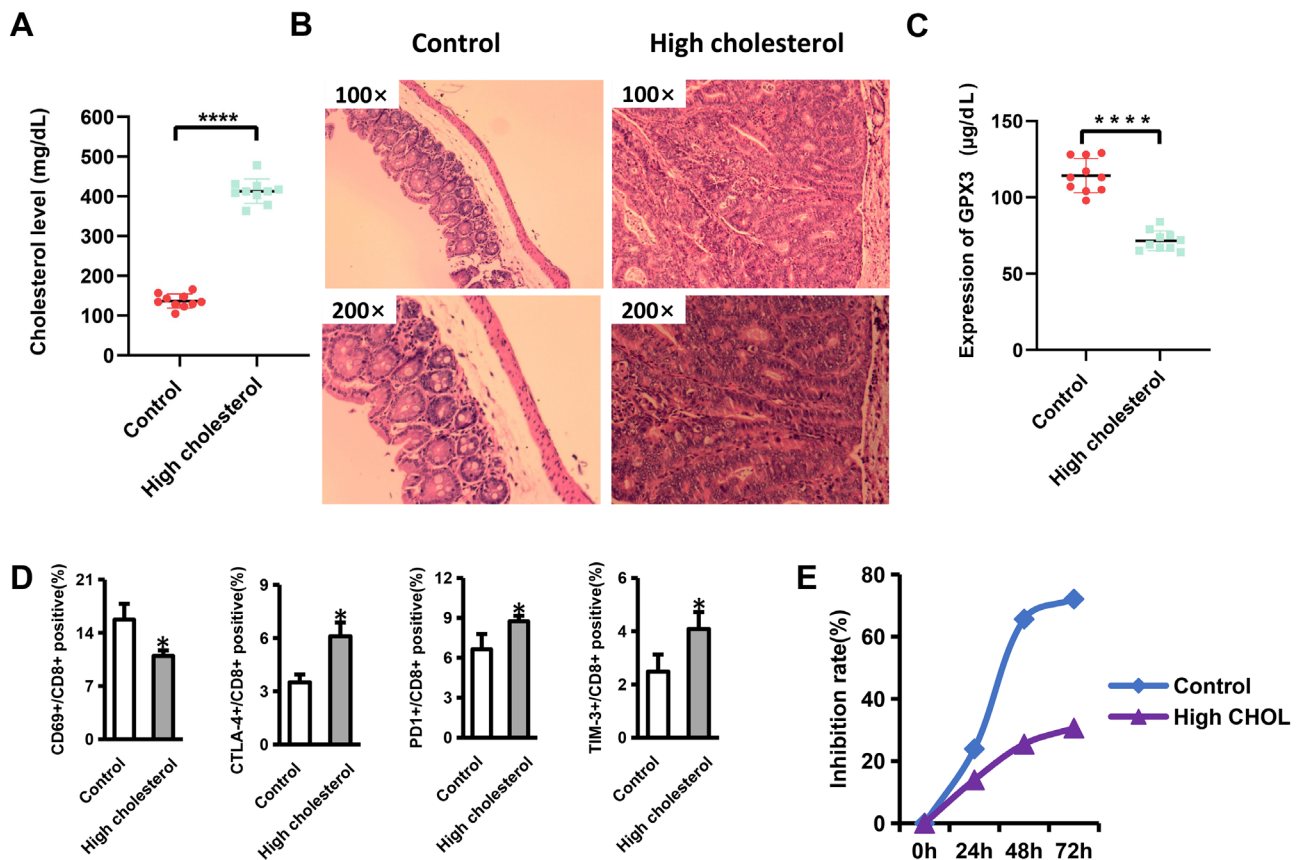


Figure 3. Cholesterol-induced CD8⁺ T cell exhaustion in mice. A) Enzymatic determination of cholesterol in the peripheral blood samples of high cholesterol mice and control mice. B) H&E-stained section of high cholesterol mice and control mice colonic tissue under 100× and 200× microscope. C) ELISA of GPX3 in the peripheral blood samples of high cholesterol mice and control mice. D) Flow cytometry shows the expression of CD69, PD-1, CTLA-4, and TIM-3 in the CD8⁺ T cells of high cholesterol mice. E) CCK-8 assay of cell proliferation in different groups, *p<0.05, **p<0.01, ***p<0.005, ****p<0.001

(Figure 5D). Several ceRNAs were identified, such as chr22-38_28785274-29006793.1/hsa-miR-507/ACTC1, chr22-38_28785274-29006793.1/hsa-miR-298/FN1, and chr22-38_28785274-29006793.1/hsa-miR-1290/SERPINE1.

Discussion

In the present study, the regulatory mechanism of cholesterol in CRC development was investigated. GPX3 was

identified as a cholesterol-related DEG that was associated with prognosis in CRC. The expression of GPX3 is downregulated in CRC and inversely correlated with cholesterol levels. CD8⁺ T cell exhaustion was also observed in high cholesterol levels. Moreover, 53 DEGs between the GPX3 high- and low-expression groups were found to be associated with m6A modification and tumor-infiltrating T cells. The T cell immune-related ceRNA network was constructed, including 7 lncRNAs, 39 miRNAs, 7 immune-related genes,

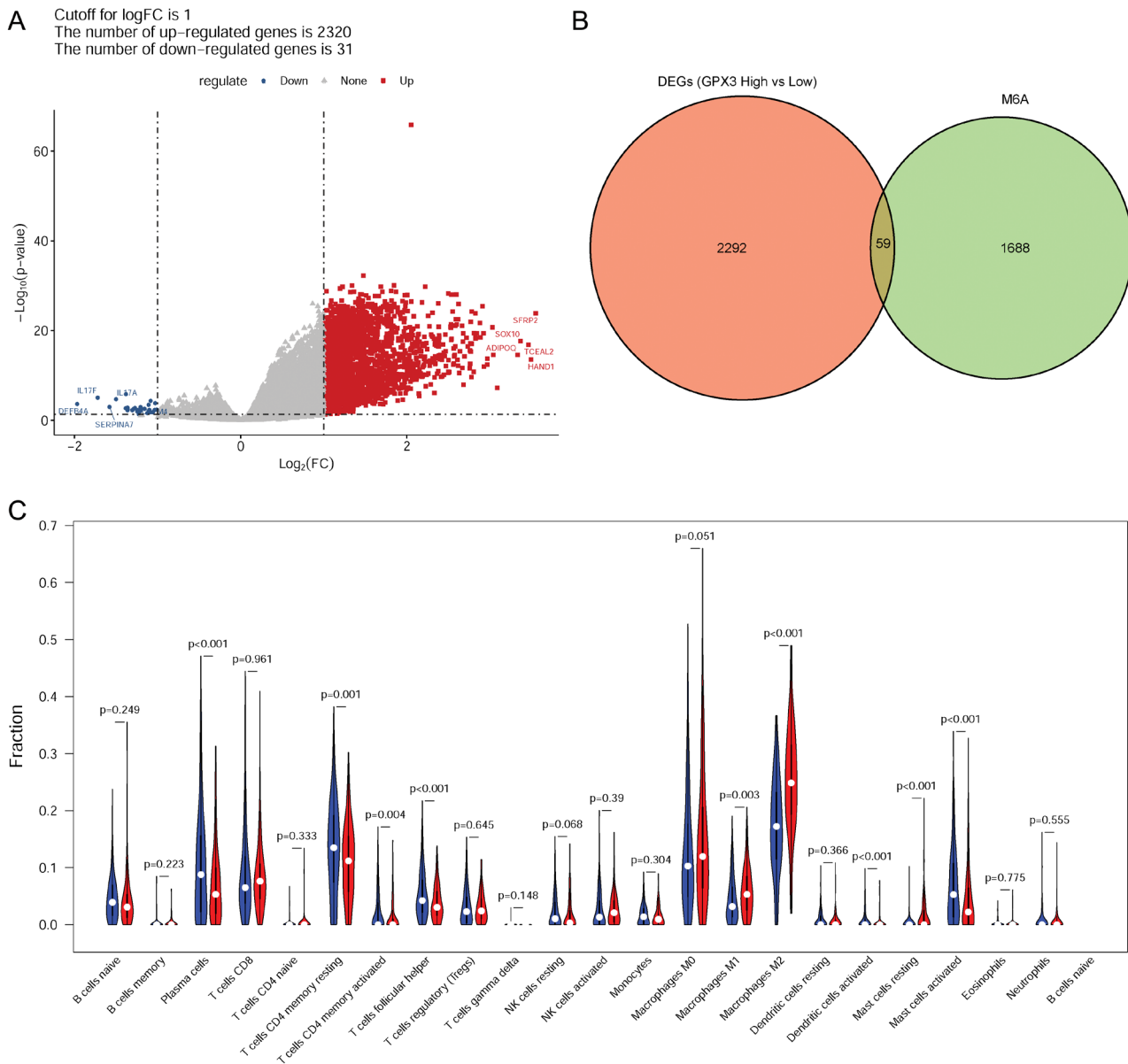


Figure 4. Analysis of GPX3-related DEGs. A) Volcano plot of DEGs between the GPX3 high- and low-expression groups. The red node represents upregulated mRNAs, and the blue node represents downregulated mRNAs. The abscissa axis is log2FC, and the longitudinal axis is log10 (p-value). B) Venn analysis shows the intersection of DEGs and m6A target genes. C) Violin plot of the abundance of 22 types of infiltrating immune cells in tumor tissues. The red indicates the high-expression group, and the blue indicates the low-expression group. Abbreviation: DEGs-differentially expressed genes.

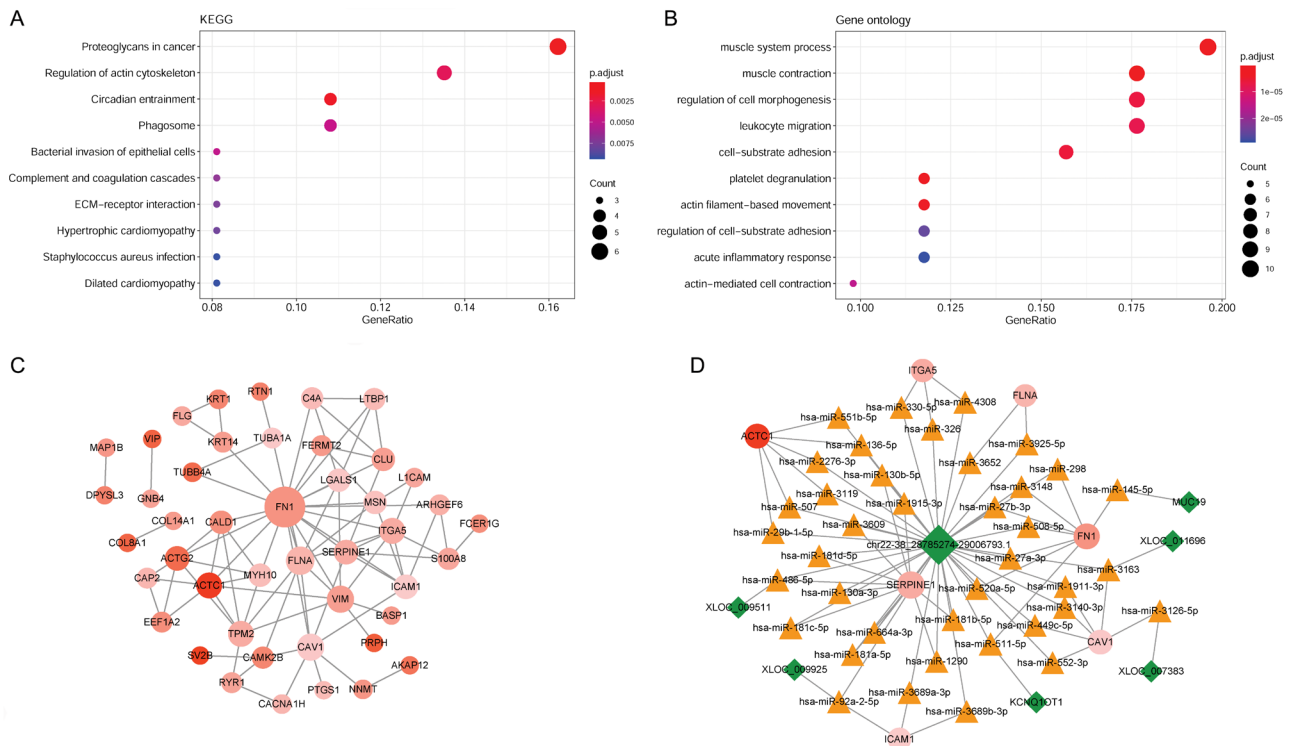


Figure 5. Functional enrichment analysis, PPI network analysis, and ceRNA network analysis for T cell immune-related genes. A) Top 10 KEGG pathway enrichment results. B) Top 10 GO BP pathway enrichment results. C) PPI network constructed with T cell immune-related genes. The darker the red node is, the greater the value of logFC is. The node size indicates the degree of connection. D) T cell immune-related ceRNA network. Green diamond nodes are lncRNAs, orange triangle nodes are miRNAs, and red circle nodes are mRNAs. The darker the red node is, the greater the value of logFC is. The grey lines represent regulatory relationships. The node size indicates the degree of connection. Abbreviations: KEGG-Kyoto Encyclopedia of Genes and Genomes; GOBP-Gene Ontology biological process; PPI-protein-protein interaction; ceRNA-competing endogenous RNA

39 miRNA-target gene pairs, and 43 lncRNA-miRNA regulatory relationships.

High cholesterol may be responsible for the development of cancer. Additionally, the expressions of GPX3 protein in CRC cancerous tissues with different stages, degrees of differentiation, and Ki-67 proliferation index were focused on. A more interesting thing was that low GPX3 expression in cancerous tissues predicted a better prognosis in CRC. At present, most studies have shown that low expression of GPX3 and high GPX3 methylation predicted poor prognosis of cancer, such as breast cancer [37], gallbladder cancer [38], and cervical cancer [39]. The specific role of GPX3 in the prognosis of CRC has not been clarified. The effects of GPX3 expression on cancer prognosis may be related to chemotherapy drug sensitivity and cancer histological type. For example, Pelosof et al. detected GPX3 methylation and expression levels in CRC tissues, and they found that increased GPX3 methylation levels in CRC tissues resulted in decreased GPX3 expression, and increased sensitivity to oxaliplatin and cisplatin [40]. By comparing the expression level and methylation of GPX3 of cancerous tissues in aggressive phenotype inflammatory breast cancer (IBC) and

non-IBC invasive ductal carcinoma (IDC), Mohamed et al. discovered that the level of GPX3 hypermethylation was lower and the expression of GPX3 was higher in IDC [41]. Patients with malignant tumors are at high risk of malnutrition. Cancer malnutrition affects disease prognosis and reduces overall survival. A prospective study enrolled 551 cancer patients who were followed for an average of 41 months, which ultimately revealed that the total cholesterol levels were significantly lower in patients who died of cancer compared with those who survived [42]. Cholesterol is not only a precursor of various hormones and bile acids but also plays an important role in the structure of cell membranes. Low cholesterol levels in cancer patients suggest a more active stage of the disease, and patients with low serum cholesterol levels may also predict a poor prognosis. Further studies are needed to explore the mechanisms of cholesterol and GPX3 in CRC development and prognosis.

The exhaustion of CD8⁺ T cells is a major factor in cancer progression and prognosis. The regulation of aerobic glycolysis, glutaminolysis, and mitochondria-related functions such as oxidative phosphorylation (OXPHOS) and single-carbon metabolism support effector CD8⁺ T cells T-cell

responses [43]. Based on Ma et al., cholesterol levels in tumor tissues are higher than in other immune organs. The higher the cholesterol content of immune cells is, the higher the expression of PD-1, LAG-3, TIM-3, 2B4, and other immune checkpoints is. Furthermore, they identified mechanisms by which high cholesterol activates the endoplasmic reticulum stress response and the IRE1 α (IRE1 α)-X box binding protein-1 (XBP1) signaling pathway to induce inhibitory receptor expression and CD8⁺ T cells exhaustion [44]. The latest study by Ma et al. proved that cholesterol in the tumor environment could induce an increase in CD36 expression in CD8⁺ T cells, which leads to excessive fatty acid intake. In the end, CD8⁺ T cells were damaged by lipid oxidation and iron-death and lost their killer function to promote tumor growth [45]. In the present study, the expression of immunosuppressants PD-1, CTLA-4, and TIM-3 was also higher in the high cholesterol level, while CD69 was lower. In addition, CD8⁺ T cell exhaustion was also observed in high cholesterol level. Interestingly, Giacomelli et al. illustrated that cell exhaustion phenotypes, such as the co-expression of PD-1 and TIM-3, were also detected in a portion of tumor-infiltrating T cells in mismatch repair proficient CRC (CRCpMMR) [46]. In contrast, PD-L1 expression was not detected in some fresh tumor cells and TAMs even after *in vitro* interferon- γ stimulation. These findings provide evidence to support the revelation of a unique immunosuppressive microenvironment in CRC. At the same time, it also suggests that the immune escape mechanism should be considered when studying the mechanism of cholesterol-induced CRC, especially the role of potential target GPX3.

Dysregulated m6A modification of key genes plays a key role in tumor development, prognosis, and TME [47]. The aberrant regulation of m6A modification in mRNAs has been implicated in the development and metastasis of CRC [41]. m6A regulators and m6A-related RNAs are considered to be promising prognostic predictors and therapeutic targets for CRC [48]. Moreover, m6A modification may be involved in TME formation in colon cancer [49]. It has been reported that tumor-infiltrating immune cells are correlated with cancer development and prognosis in patients with CRC [50]. Moreover, tumor-infiltrating T cells have been suggested to be the biological basis of immunotherapy and serve as promising predictors of cancer prognosis [51]. To further investigate the downstream regulatory mechanism of GPX3, key GPX3 downstream genes associated with m6A modification and tumor-infiltrating T cells were identified, such as FN1, ACTC1, and SERPINE1, which are hub nodes in both the PPI network and the ceRNA network. It has been shown that FN1 (fibronectin 1) has key functions in cellular adhesion and migration processes [52]. FN1/SPP1-ITGAV signaling is activated in the fibrotic microenvironment and consequently promotes the metastatic seeding of CRC [53, 54]. ACTC1 (actin alpha cardiac muscle 1) is an actin family member implicated in cell motility. Patients with ACTC1-positive glioblastomas have a poorer prognosis than those

with ACTC1-negative glioblastomas, which suggests the potential of ACTC1 as an invasion and prognosis marker in glioblastoma [55]. SERPINE1 (serpin family E member 1) is the main inhibitor of the urokinase plasminogen activator/urokinase plasminogen activator receptor (uPA/uPAR) complex and plays a key role in regulating the adhesion/de-adhesion balance of cells to the extracellular matrix, thus affecting tumor cell migration [56]. SERPINE1 expression is associated with an increased risk of metastasis and poor outcome [57]. Notably, SERPINE1 plays a role in immune cell infiltration and TME remodeling, thus affecting the process of CRC development [58]. Our results revealed that these T cell immune-related genes were enriched in migration-related pathways, such as leukocyte migration and cell-substrate adhesion. Therefore, it is believed that GPX3 may affect the metastasis and TME of CRC by regulating the expression of these genes associated with m6A modification and tumor-infiltrating T cells. These genes may serve as promising targets for immunotherapy in patients with CRC.

Non-coding RNAs (ncRNAs), such as miRNAs and lncRNAs, have been implicated in the proliferation and metastasis of various cancers [59]. ceRNA networks have been established to associate the function of protein-coding mRNAs with ncRNAs, such as miRNAs and lncRNAs [60]. Consistent with previous findings that chr22-38_28785274-29006793.1 is related to CD4⁺ and CD8⁺ T cell infiltration in colon cancer [61], this study also proved that chr22-38_28785274-29006793.1 could interact with the greatest number of miRNAs in our constructed ceRNA network. Moreover, it has been shown that the lncRNA LINC00525 enhances stemness properties and chemoresistance in CRC by targeting the miR-507/ELK3 axis [62], which suggests a potential role of miR-507 in CRC. It has been found that miR-298 is correlated with the cancer development and overall survival of patients with CRC [63]. It has been reported that miR-1290 participates in CRC development and may serve as a promising target for cancer diagnosis and prognosis [64, 65]. Based on our results, hub nodes, such as FN1, ACTC1, and SERPINE1, were identified in the ceRNA network, and they may be associated with T cell infiltration in CRC and contribute to the immune escape of tumors. Despite the lack of further molecular confirmation, our findings may provide directions for future research on tumor immunity.

Admittedly, although this study displayed that cholesterol may regulate T cells through GPX3 in CRC, the specific regulatory mechanism is still unclear, and in-depth mechanism studies need to be carried out to clarify the role of GPX3 in regulating T cell immunity. Furthermore, it was clear that GPX3 is an important target affecting prognosis, but the included clinical sample size may be insufficient. Multicenter, large sample clinical samples need to be included to further verify the value of GPX3 in prognosis. In the high-cholesterol group samples, a distinct population of cells with higher FSC and SSC was observed, absent in the control group,

prompting the need for further research to understand their role in disease.

In conclusion, the cholesterol-related gene GPX3 is a key molecule in the regulation of colorectal cancer T cells. The expression of GPX3 was negatively associated with cholesterol level but positively correlated with the Ki-67 proliferation index. The expression of GPX3 was higher in poorly differentiated and advanced stage. Besides, high cholesterol can induce CD8⁺ T cells exhaustion. In summary, as a new target of cholesterol regulation of CRC, GPX3 is expected to provide new ideas for explaining the pathogenesis of CRC from the perspective of immunity.

Supplementary information is available in the online version of the paper.

Acknowledgments: This research was supported by the Public Welfare Technology Application Research Program of Huzhou (2021GY05), the Medical and Health Technology Project of Zhejiang Province (No.2022KY1220, No.2023KY1170), and the Natural Science Foundation of Zhejiang Province (No. LQ23H160006). The authors gratefully acknowledge the database available to us for this study. Meanwhile, we thank the patients and volunteers for their contributions to the sample collection.

References

- [1] BRAY F, FERLAY J, SOERJOMATARAM I, SIEGEL RL, TORRE LA et al. Global cancer statistics 2018: GLOBOCAN estimates of incidence and mortality worldwide for 36 cancers in 185 countries. *CA Cancer J Clin* 2018; 68: 394–424. <https://doi.org/10.3322/caac.21609>
- [2] ALLEMANI C, MATSUDA T, DI CARLO V, HAREWOOD R, MATZ M et al. Global surveillance of trends in cancer survival 2000–14 (CONCORD-3): analysis of individual records for 37 513 025 patients diagnosed with one of 18 cancers from 322 population-based registries in 71 countries. *Lancet* 2018; 391: 1023–1075. [https://doi.org/10.1016/S0140-6736\(17\)33326-3](https://doi.org/10.1016/S0140-6736(17)33326-3)
- [3] MONTALBAN-ARQUES A, SCHARL M. Intestinal microbiota and colorectal carcinoma: Implications for pathogenesis, diagnosis, and therapy. *EBioMedicine* 2019; 48: 648–655. <https://doi.org/10.1016/j.ebiom.2019.09.050>
- [4] KUZU OF, NOORY MA, ROBERTSON GP. The Role of Cholesterol in Cancer. *Cancer Res* 2016; 76: 2063–2070. <https://doi.org/10.1158/0008-5472.CAN-15-2613>
- [5] MURAI T. Cholesterol lowering: role in cancer prevention and treatment. *Biol Chem* 2015; 396: 1–11. <https://doi.org/10.1515/hsz-2014-0194>
- [6] GARCIA-ESTEVEZ L, MORENO-BUENO G. Updating the role of obesity and cholesterol in breast cancer. *Breast Cancer Res* 2019; 21: 1019–1124. <https://doi.org/10.1186/s13058-019-1124-1>
- [7] WANG C, LI P, XUAN J, ZHU C, LIU J et al. Cholesterol Enhances Colorectal Cancer Progression via ROS Elevation and MAPK Signaling Pathway Activation. *Cell Physiol Biochem* 2017; 42: 729–742. <https://doi.org/10.1159/000477890>
- [8] JUN SY, BROWN AJ, CHUA NK, YOON JY, LEE JJ et al. Reduction of Squalene Epoxidase by Cholesterol Accumulation Accelerates Colorectal Cancer Progression and Metastasis. *Gastroenterology* 2021; 160: 1194–1207. <https://doi.org/10.1053/j.gastro.2020.09.009>
- [9] VASSILEV B, SIHTO H, LI S, HÖLTTÄ-VUORI M, ILOLA J et al. Elevated levels of StAR-related lipid transfer protein 3 alter cholesterol balance and adhesiveness of breast cancer cells: potential mechanisms contributing to progression of HER2-positive breast cancers. *Am J Pathol* 2015; 185: 987–1000. <https://doi.org/10.1016/j.ajpath.2014.12.018>
- [10] DENG W, LIU H, LUO S, CLARKE J, GLASS C et al. APOB Genotypes and CDH13 Haplotypes in the Cholesterol-Related Pathway Genes Predict Non-Small Cell Lung Cancer Survival. *Cancer Epidemiol Biomarkers Prev* 2020; 29: 1204–1213. <https://doi.org/10.1158/1055-9965.EPI-19-1262>
- [11] SHARMA B, GUPTA V, DAHIYA D, KUMAR H, VAIPHEI K et al. Clinical relevance of cholesterol homeostasis genes in colorectal cancer. *Biochim Biophys Acta Mol Cell Biol Lipids* 2019; 10: 13. <https://doi.org/10.1016/j.bbalip.2019.06.008>
- [12] MAITY A, DAS B. N6-methyladenosine modification in mRNA: machinery, function and implications for health and diseases. *FEBS J* 2016; 283: 1607–1630. <https://doi.org/10.1111/febs.13614>
- [13] LIN X, CHAI G, WU Y, LI J, CHEN F et al. RNA m(6)A methylation regulates the epithelial mesenchymal transition of cancer cells and translation of Snail. *Nat Commun* 2019; 10: 2065. <https://doi.org/10.1038/s41467-019-09865-9>
- [14] LIU J, ECKERT MA, HARADA BT, LIU SM, LU Z et al. m(6)A mRNA methylation regulates AKT activity to promote the proliferation and tumorigenicity of endometrial cancer. *Nat Cell Biol* 2018; 20: 1074–1083. <https://doi.org/10.1038/s41556-018-0174-4>
- [15] LIU X, LIU L, DONG Z, LI J, YU Y et al. Expression patterns and prognostic value of m(6)A-related genes in colorectal cancer. *Am J Transl Res* 2019; 11: 3972–3991.
- [16] TANG R, ZHANG Y, LIANG C, XU J, MENG Q et al. The role of m6A-related genes in the prognosis and immune microenvironment of pancreatic adenocarcinoma. *PeerJ* 2020; 8: e9602. <https://doi.org/10.7717/peerj.9602>
- [17] LEI X, LEI Y, LI JK, DU WX, LI RG et al. Immune cells within the tumor microenvironment: Biological functions and roles in cancer immunotherapy. *Cancer Lett* 2020; 470: 126–133. <https://doi.org/10.1016/j.canlet.2019.11.009>
- [18] MA X, BI E, LU Y, SU P, HUANG C et al. Cholesterol Induces CD8(+) T Cell Exhaustion in the Tumor Microenvironment. *Cell Metab* 2019; 30: 143–156.e5. <https://doi.org/10.1016/j.cmet.2019.04.002>
- [19] GE P, WANG W, LI L, ZHANG G, GAO Z et al. Profiles of immune cell infiltration and immune-related genes in the tumor microenvironment of colorectal cancer. *Biomed Pharmacother* 2019; 118: 109228. <https://doi.org/10.1016/j.biopha.2019.109228>
- [20] BAEK AE, YU YA, HE S, WARDELL SE, CHANG CY et al. The cholesterol metabolite 27 hydroxycholesterol facilitates breast cancer metastasis through its actions on immune cells. *Nat Commun* 2017; 8: 864. <https://doi.org/10.1038/s41467-017-00910-z>

- [21] SAG D, CEKIC C, WU R, LINDEN J, HEDRICK CC. The cholesterol transporter ABCG1 links cholesterol homeostasis and tumour immunity. *Nat Commun* 2015; 6: 6354. <https://doi.org/10.1038/ncomms7354>
- [22] ROSENBLOOM KR, ARMSTRONG J, BARBER GP, CASPER J, CLAWSON H et al. The UCSC Genome Browser database: 2015 update. *Nucleic Acids Res* 2015; 43: D670–681. <https://doi.org/10.1093/nar/gku1177>
- [23] HARROW J, FRANKISH A, GONZALEZ JM, TAPANARI E, DIEKHANS M et al. GENCODE: the reference human genome annotation for The ENCODE Project. *Genome Res* 2012; 22: 1760–1774. <https://doi.org/10.1101/gr.135350.111>
- [24] SMYTH GK. *limma: Linear Models for Microarray Data*. In: Gentleman R, Carey VJ, Huber W, Irizarry RA, Dudoit S (Eds.). *Bioinformatics and Computational Biology Solutions Using R and Bioconductor*. Springer International Publishing, New York 2005, p. 397–420.
- [25] THERNEAU TM, GRAMBSCHE MP. *Modeling Survival Data: Extending the Cox Model*. Springer. Springer Science & Business Media ISBN 0-387-98784-3
- [26] LIU L, GAO H, WEN T, GU T, ZHANG S et al. Tanshinone IIA attenuates AOM/DSS-induced colorectal tumorigenesis in mice via inhibition of intestinal inflammation. *Pharm Biol* 2021; 59: 89–96. <https://doi.org/10.1080/13880209.2020.1865412>
- [27] NEWMAN AM, LIU CL, GREEN MR, GENTLES AJ, FENG W et al. Robust enumeration of cell subsets from tissue expression profiles. *Nature Methods* 2015; 12: 453–457. <https://doi.org/10.1038/nmeth.3337>
- [28] KANEHISA M, GOTO S. KEGG: Kyoto Encyclopedia of Genes and Genomes. *Nucleic Acids Research* 2000; 28: 27–30. <https://doi.org/10.1093/nar/28.1.27>
- [29] CARBON S, DOUGLASS E, DUNN N, GOOD BM, HARRIS NL et al. The Gene Ontology Resource: 20 years and still GOing strong. *Nucleic Acids Res* 2019; 47: D330–338. <https://doi.org/10.1093/nar/gky1055>
- [30] YU G, WANG LG, HAN Y, HE QY. clusterProfiler: an R package for comparing biological themes among gene clusters. *OMICS* 2012; 16: 284–287. <https://doi.org/10.1089/omi.2011.0118>
- [31] SZKLARCZYK D, FRANCESCHINI A, WYDER S, FORSLUND K, HELLER D et al. STRING v10: protein–protein interaction networks, integrated over the tree of life. *Nucleic Acids Res* 2015; 43: D447–452. <https://doi.org/10.1093/nar/gku1003>
- [32] OTASEK D, MORRIS JH, BOUCAS J, PICO AR, DEMCHAK B. Cytoscape Automation: empowering workflow-based network analysis. *Genome Biol* 2019; 20: 185. <https://doi.org/10.1186/s13059-019-1758-4>
- [33] BREUER K, FOROUSHANI AK, LAIRD MR, CHEN C, SRIBNAIA A et al. InnateDB: systems biology of innate immunity and beyond--recent updates and continuing curation. *Nucleic Acids Res* 2013; 41: D1228–1233. <https://doi.org/10.1093/nar/gks1147>
- [34] DWEEP H, GRETZ N. miRWalk2. 0: a comprehensive atlas of microRNA-target interactions. *Nat Methods* 2015; 12: 697. <https://doi.org/10.1038/nmeth.3485>
- [35] PARASKEVOPOULOU M, VLACHOS I, KARAGKOUNI D, GEORGAKILAS G, KANELLOS I et al. DIANA-Lnc-Base v2: indexing microRNA targets on non-coding transcripts. *Nucleic Acids Res* 2016; 44: D231–238. <https://doi.org/10.1093/nar/gkv1270>
- [36] TANG Y, LI M, WANG J, PAN Y, WU FX. CytoNCA: a cytoscape plugin for centrality analysis and evaluation of biological networks. *Biosystems* 2014; 11: 67–72. <https://doi.org/10.1016/j.biosystems.2014.11.005>
- [37] LOU W, DING B, WANG S, FU P. Overexpression of GPX3, a potential biomarker for diagnosis and prognosis of breast cancer, inhibits progression of breast cancer cells in vitro. *Cancer Cell Int* 2020; 20: 378. <https://doi.org/10.1186/s12935-020-01466-7>
- [38] YANG ZL, YANG L, ZOU Q, YUAN Y, LI J et al. Positive ALDH1A3 and negative GPX3 expressions are biomarkers for poor prognosis of gallbladder cancer. *Dis Markers* 2013; 35: 163–172. <https://doi.org/10.1155/2013/187043>
- [39] ZHANG X, ZHENG Z, YINGJI S, KIM H, JIN R et al. Downregulation of glutathione peroxidase 3 is associated with lymph node metastasis and prognosis in cervical cancer. *Oncol Rep* 2014; 31: 2587–2592. <https://doi.org/10.3892/or.2014.3152>
- [40] PELOSOF L, YERRAM S, ARMSTRONG T, CHU N, DANILOVA L et al. GPX3 promoter methylation predicts platinum sensitivity in colorectal cancer. *Epigenetics* 2017; 12: 540–550. <https://doi.org/10.1080/15592294.2016.1265711>
- [41] MOHAMED MM, SABET S, PENG DF, NOUH MA, EL-SHINAWI M et al. Promoter hypermethylation and suppression of glutathione peroxidase 3 are associated with inflammatory breast carcinogenesis. *Oxid Med Cell Longev* 2014; 2014: 787195. <https://doi.org/10.1155/2014/787195>
- [42] HOHNECK AL, ROSENKAIMER S, HOFHEINZ RD, AKIN I, BORGGREFE M et al. Blood Cholesterol and Outcome of Patients with Cancer under Regular Cardiological Surveillance. *Curr Oncol* 2021; 28: 863–872. <https://doi.org/10.3390/curroncol28010085>
- [43] LEONE RD, POWELL JD. Fueling the Revolution: Targeting Metabolism to Enhance Immunotherapy. *Cancer Immunol Res* 2021; 9: 255–260. <https://doi.org/10.1158/2326-6066.CIR-20-0791>
- [44] MA X, BIE E, LU Y, SU P, HUANG C et al. Cholesterol Induces CD8+ T Cell Exhaustion in the Tumor Microenvironment. *Cell Metab* 2019; 30: 143–156.e5. <https://doi.org/10.1016/j.cmet.2019.04.002>
- [45] MA X, XIAO L, LIU L, YE L, SU P et al. CD36-mediated ferroptosis dampens intratumoral CD8+ T cell effector function and impairs their antitumor ability. *Cell Metab* 2021; 33: 1001–1012.e5. <https://doi.org/10.1016/j.cmet.2021.02.015>
- [46] GIACOMELLI M, MONTI M, PEZZOLA DC, LONARDI S, BUGATTI M et al. Immuno-Contexture and Immune Checkpoint Molecule Expression in Mismatch Repair Proficient Colorectal Carcinoma. *Cancers (Basel)* 2023; 15: 3097. <https://doi.org/10.3390/cancers15123097>

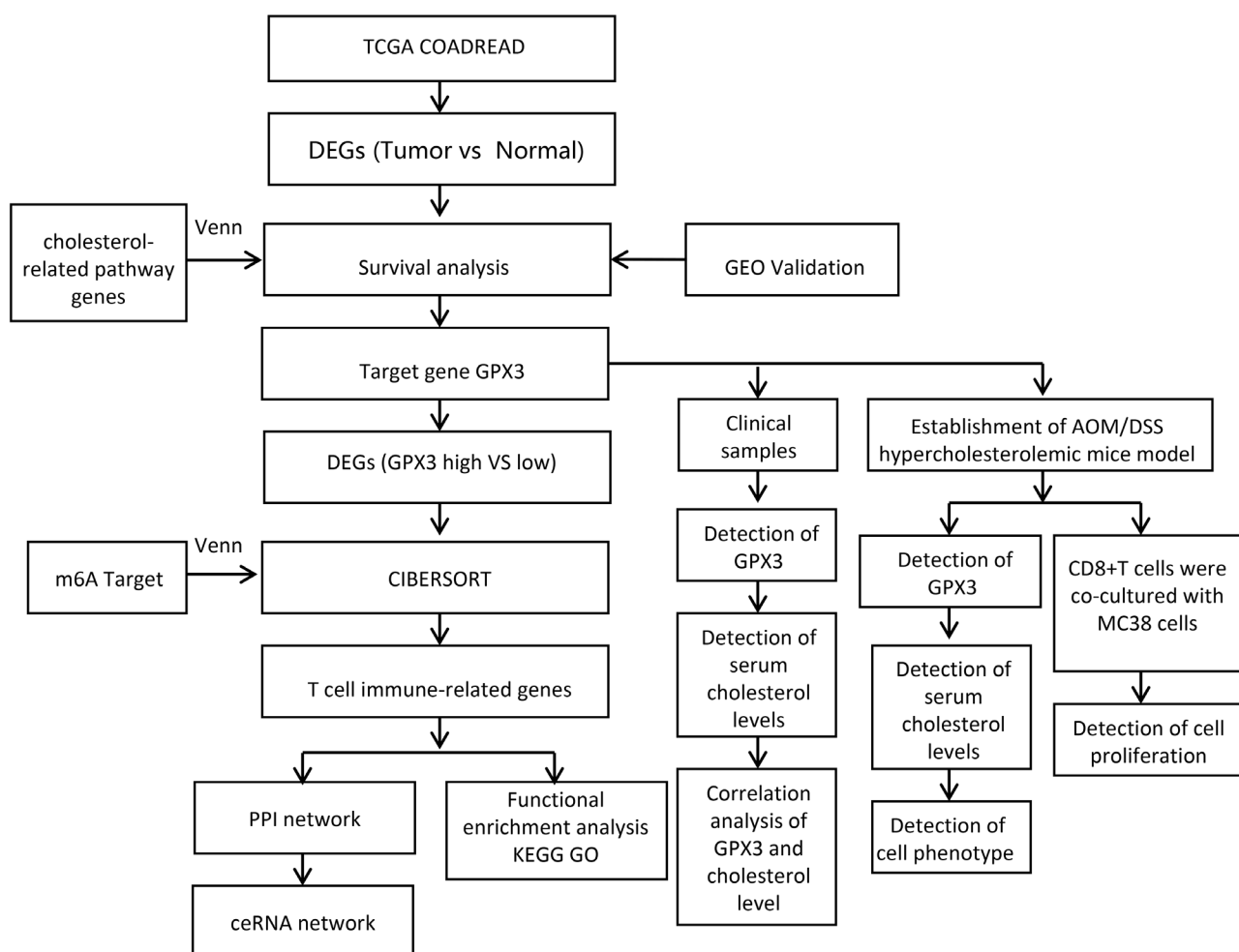
- [47] XU F, ZHANG Z, YUAN M, ZHAO Y, ZHOU Y et al. M6A Regulatory Genes Play an Important Role in the Prognosis, Progression and Immune Microenvironment of Pancreatic Adenocarcinoma. *Cancer Invest* 2021; 39: 39–54. <https://doi.org/10.1080/07357907.2020.1834576>
- [48] LI J, LIANG L, YANG Y, LI X, MA Y. N(6)-methyladenosine as a biological and clinical determinant in colorectal cancer: progression and future direction. *Theranostics* 2021; 11: 2581–2593. <https://doi.org/10.7150/thno.52366>
- [49] CHONG W, SHANG L, LIU J, FANG Z, DU F et al. m(6) A regulator-based methylation modification patterns characterized by distinct tumor microenvironment immune profiles in colon cancer. *Theranostics* 2021; 11: 2201–2217. <https://doi.org/10.7150/thno.52717>
- [50] YE L, ZHANG T, KANG Z, GUO G, SUN Y et al. Tumor-Infiltrating Immune Cells Act as a Marker for Prognosis in Colorectal Cancer. *Front Immunol* 2019; 10: 2368. <https://doi.org/10.3389/fimmu.2019.02368>
- [51] WANG W, ZOU W, LIU JR. Tumor-infiltrating T cells in epithelial ovarian cancer: predictors of prognosis and biological basis of immunotherapy. *Gynecologic Oncol* 2018; 151: 1–3. <https://doi.org/10.1016/j.ygyno.2018.09.005>
- [52] GAO W, LIU Y, QIN R, LIU D, FENG Q. Silence of fibronectin 1 increases cisplatin sensitivity of non-small cell lung cancer cell line. *Biochem Biophys Res Commun* 2016; 476: 35–41. <https://doi.org/10.1016/j.bbrc.2016.05.081>
- [53] ZHANG C, WU M, ZHANG L, SHANG LR, FANG JH et al. Fibrotic microenvironment promotes the metastatic seeding of tumor cells via activating the fibronectin 1/secreted phosphoprotein 1-integrin signaling. *Oncotarget* 2016; 7: 45702–45714. <https://doi.org/10.18632/oncotarget.10157>
- [54] CAI X, LIU C, ZHANG TN, ZHU YW, DONG X et al. Down-regulation of FN1 inhibits colorectal carcinogenesis by suppressing proliferation, migration, and invasion. *J Cell Biochem* 2018; 119: 4717–4728. <https://doi.org/10.1002/jcb.26651>
- [55] OHTAKI S, WANIBUCHI M, KATAOKA-SASAKI Y, SASAKI M, OKA S et al. ACTC1 as an invasion and prognosis marker in glioma. *J Neurosurg* 2017; 126: 467–475. <https://doi.org/10.3171/2016.1.JNS152075>
- [56] SIMONE TM, LONGMATE WM, LAW BK, HIGGINS PJ. Targeted Inhibition of PAI-1 Activity Impairs Epithelial Migration and Wound Closure Following Cutaneous Injury. *Adv Wound Care (New Rochelle)* 2015; 4: 321–328. <https://doi.org/10.1089/wound.2014.0611>
- [57] DUFFY MJ, MCGOWAN PM, GALLAGHER WM. Cancer invasion and metastasis: changing views. *J Pathol* 2008; 214: 283–293. <https://doi.org/10.1002/path.2282>
- [58] WANG S, PANG L, LIU Z, MENG X. SERPINE1 associated with remodeling of the tumor microenvironment in colon cancer progression: a novel therapeutic target. *BMC Cancer* 2021; 21: 767. <https://doi.org/10.1186/s12885-021-08536-7>
- [59] ESMAEILI M, KESHANI M, VAKILIAN M, PEYMANI M, SEYED FOROOTAN F et al. Role of non-coding RNAs as novel biomarkers for detection of colorectal cancer progression through interaction with the cell signaling pathways. *Gene* 2020; 753: 144796. <https://doi.org/10.1016/j.gene.2020.144796>
- [60] QI X, ZHANG DH, WU N, XIAO JH, WANG X et al. ceRNA in cancer: possible functions and clinical implications. *J Med Genet.* 2015; 52: 710–718. <https://doi.org/10.1136/jmedgenet-2015-103334>
- [61] YANG X, WU W, PAN Y, ZHOU Q, XU J et al. Immune-related genes in tumor-specific CD4(+) and CD8(+) T cells in colon cancer. *BMC Cancer* 2020; 20: 585. <https://doi.org/10.1186/s12885-020-07075-x>
- [62] WANG S, LI J, YANG X. Long Non-Coding RNA LINC00525 Promotes the Stemness and Chemoresistance of Colorectal Cancer by Targeting miR-507/ELK3 Axis. *Int J Stem Cells* 2019; 12: 347–359. <https://doi.org/10.15283/ijsc19041>
- [63] ARABSORKHI Z, GHARIB E, YAGHMOORIAN KHOJINI J, FARHADIEH ME, NAZEMALHOSSEINI-MOJARAD E et al. miR-298 plays a pivotal role in colon cancer invasiveness by targeting PTEN. *J Cell Physiol* 2020; 235: 4335–4350. <https://doi.org/10.1002/jcp.29310>
- [64] MA Q, WANG Y, ZHANG H, WANG F. miR-1290 Contributes to Colorectal Cancer Cell Proliferation by Targeting INPP4B. *Oncol Res* 2018; 26: 1167–1174. <https://doi.org/10.3727/096504017X15051741798389>
- [65] IMAOKA H, TOIYAMA Y, FUJIKAWA H, HIRO J, SAIGUSA S et al. Circulating microRNA-1290 as a novel diagnostic and prognostic biomarker in human colorectal cancer. *Ann Oncol* 2016; 27: 1879–1186. <https://doi.org/10.1093/annonc/mdw279>

https://doi.org/10.4149/neo_2023_230704N348

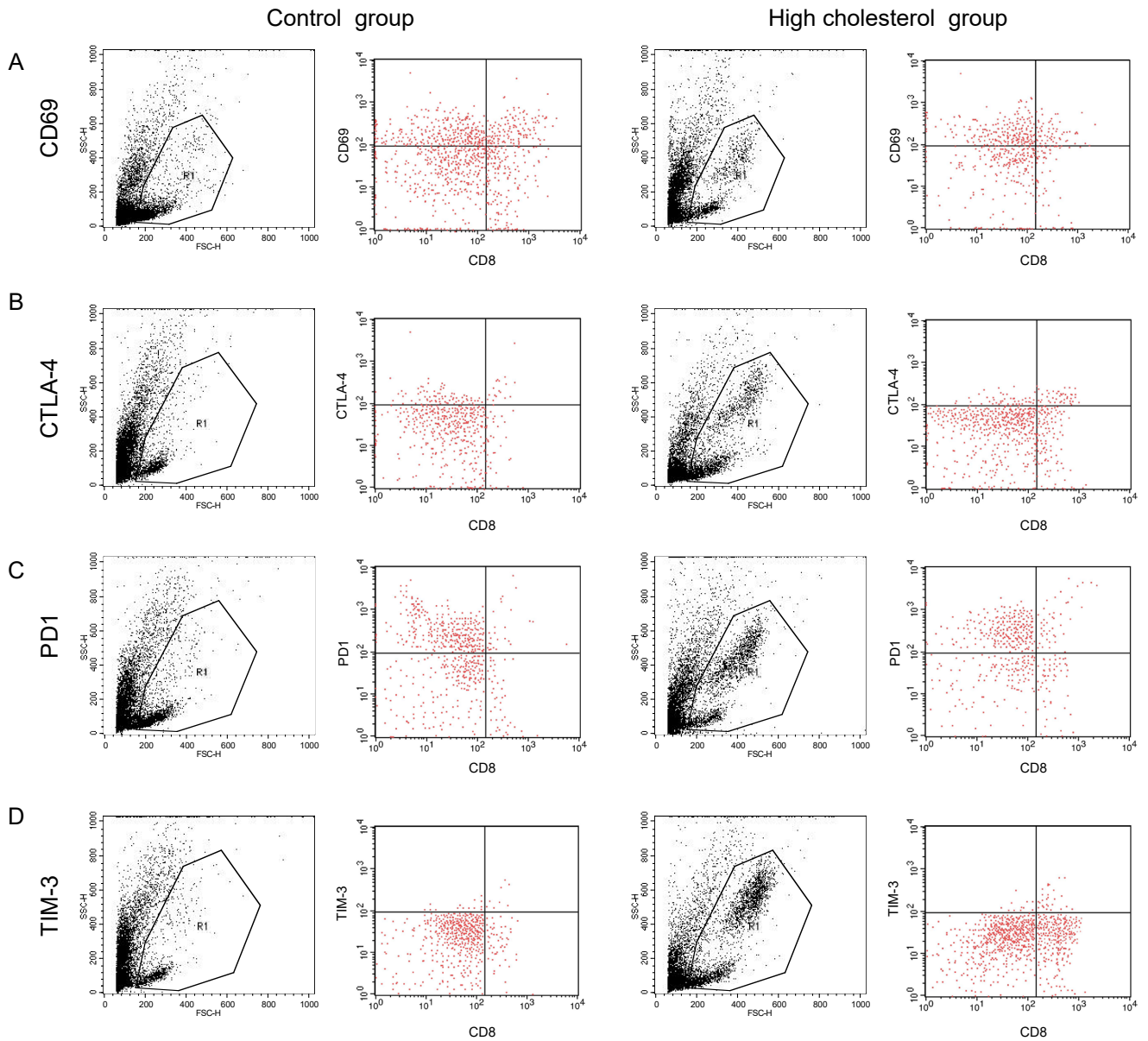
GPX3 is a key cholesterol-related gene associated with prognosis and tumor-infiltrating T cells in colorectal cancer

Jiming CHEN^{1,2,3}, Yinhang WU^{1,2,3}, Qing ZHOU^{1,2,3}, Yifei SONG^{1,2,3}, Jing ZHUANG^{1,2,3}, Kongjie LU^{1,2,3,*}, Xi YANG^{1,2,3,*}

Supplementary Information



Supplementary Figure S1. Flowchart of the study.



Supplementary Figure S2: Flow cytometry shows the expression of CD69, PD-1, CTLA-4, and TIM-3 in the CD8+ T cells. A) The cell proportion in each quadrant is representative of (UL) CD69+/CD8-, (UR) CD69+/CD8+, (LL) CD69-/CD8-, and (LR) CD69-/CD8+ B) The cell proportion in each quadrant is representative of (UL) CTLA-4+/CD8-, (UR) CTLA-4+/CD8+, (LL) CTLA-4-/CD8-, and (LR) CTLA-4-/CD8+ C) The cell proportion in each quadrant is representative of (UL) PD1+/CD8-, (UR) PD1+/CD8+, (LL) PD1-/CD8-, and (LR) PD1-/CD8+ D) The cell proportion in each quadrant is representative of (UL) TIM-3+/CD8-, (UR) TIM-3+/CD8+, (LL) TIM-3-/CD8-, and (LR) TIM-3-/CD8+

Supplementary Table S1. Cholesterol-related KEGG pathways.

ID	KEGG pathways
hsa00061	Fatty acid biosynthesis
hsa00062	Fatty acid elongation
hsa00071	Fatty acid degradation
hsa00072	Synthesis and degradation of ketone bodies
hsa00100	Steroid biosynthesis
hsa00120	Primary bile acid biosynthesis
hsa00140	Steroid hormone biosynthesis
hsa00564	Glycerophospholipid metabolism
hsa00565	Ether lipid metabolism
hsa00590	Arachidonic acid metabolism
hsa00591	Linoleic acid metabolism
hsa00592	alpha-Linolenic acid metabolism
hsa00600	Sphingolipid metabolism
hsa01212	Fatty acid metabolism
hsa04920	Adipocytokine signaling pathway
hsa04923	Regulation of lipolysis in adipocytes
hsa04975	Fat digestion and absorption
hsa04979	Cholesterol metabolism
hsa01040	Biosynthesis of unsaturated fatty acids
hsa00561	Glycerolipid metabolism
hsa03320	PPAR signaling pathway